FEATURE ARTICLE

ChemComm
www.rsc.org/chemcomm

Integral atomic layer architectures of 1D crystals inserted into single walled carbon nanotubes

Jeremy Sloan,*[ab] Angus I. Kirkland,[c] John L. Hutchison[b] and Malcolm L. H. Green[a]

[a] *Inorganic Chemistry Laboratory, University of Oxford, South Parks Road, Oxford, UK OX1 3QR. E-mail: jeremy.sloan@chem.ox.ac.uk; malcolm.green@chem.ox.ac.uk*

[b] *Department of Materials, University of Oxford, Parks Road, Oxford, UK OX1 3PH. E-mail: john.hutchison@materials.ox.ac.uk*

[c] *Department of Materials Science and Metallurgy, University of Cambridge, Pembroke Street, Cambridge, UK CB2 3QZ. E-mail: aik10@cus.cam.ac.uk*

Received (in Cambridge, UK) 15th January 2002, Accepted 6th March 2002
First published as an Advance Article on the web 3rd April 2002

The crystal growth behaviour of solid phase halides encapsulated within single walled carbon nanotubes (SWNTs) is reviewed. As SWNTs form atomically thin channels within a restricted diameter range, their internal van der Waals surfaces regulate the growth behaviour of encapsulated materials in a very precise fashion. Crystal growth within SWNTs is therefore atomically regulated and nano-scale crystals with precise integral layer architectures (*i.e.* 'Feynman Crystals') can be formed. The structural properties of the resulting 1D crystals are principally dictated by the structural chemistry of the bulk material although deviations from bulk crystal growth behaviour are observed. Alternatively, 1D crystals with completely novel structures can form inside SWNTs. Where the encapsulated crystal has a structure recognizably related to that of the bulk material, crystals are formed with lower surface coordination and all exhibit substantial lattice distortions as a result of this reduced coordination and/or van der Waals constriction effects. 1D crystal growth within SWNTs is occasionally impeded by the presence of simultaneously incorporated fullerene molecules.

Introduction

In his famous address *There's Plenty of Room at the Bottom* in 1959,[1] Nobel Laureate Richard Feynman stated: 'What could we do with layered structures with just the right layers? What would the properties of materials be if we could really arrange the atoms the way we want them? They would be very interesting to investigate theoretically. I can't see exactly what would happen, but I can hardly doubt that when we have some *control* of the arrangement of things on a small scale we will get an enormously greater range of possible properties that substances can have, and of different things that we can do.' Although advances in materials fabrication technology since 1959 have made it possible to manipulate the formation of matter on an atomic scale, there are still relatively few methodologies for the production of discrete atomically regulated or 'Feynman'-type solids on a large scale. To date, some of the most successful strategies have either involved local atomistically regulated deposition of materials on solid surfaces, as in, for example, the formation of quantum dot-type structures,[2] or, alternatively, manipulation of deposited molecules and atoms *via* Atomic Force or Scanning Tunnelling Microscopy (AFM or STM).[3–9]

In the three dimensional domain, it has been possible to study the atomistically controlled formation of materials within templating structures consisting either of layered structures or of parallel aligned and ultrathin uniform channels. These structural criteria are easily met by the wide range of layered, nanoporous (*i.e.* zeolitic) or mesoporous structures that have been described in the literature.[10–14] Much work has been

Jeremy Sloan obtained his B.Sc. in Chemistry from the University of Hull in 1982, his M.Sc. in 1990 from the State University of New York at Binghamton and his Ph.D. in materials chemistry in 1995 from the University of Wales, Cardiff under the supervision of Professor Richard Tilley FRSC. He joined the Inorganic Chemistry Laboratory in 1995 as a post doctoral research assistant to Professor Malcolm Green FRS. In 2000 he was awarded a Royal Society University Research Fellowship. He is a member of Wolfson College.

Angus Kirkland graduated B.A. from the University of Cambridge in 1983 and was awarded his M.A. and Ph.D. in electron microscopy from the University of Cambridge in 1989. He then spent two years as an EPSRC research associate in the Department of Chemistry in Cambridge. In 1991 he was awarded the Ramsay Memorial Research Fellowship followed by appointment as an Isaac Newton Trust research associate in the Departments of Materials science and Chemistry in 1994 and to his current post as Senior Research Fellow in 1997. He was elected to fellowship of Fitzwilliam College, Cambridge, in 1992.

John Hutchison obtained his B.Sc. in chemistry from Glasgow University in 1967 followed by his Ph.D. in 1970. From 1970–1975 he was a postdoctoral research fellow in the Inorganic Chemistry Laboratory in Oxford and subsequently took up an appointment as a research associate at the University of Wales, Aberystwyth. In 1979 he returned to Oxford and has successively held appointments as an SERC Advanced Fellow, Senior Research Fellow and Research Lecturer. In 1999 he was promoted to Reader in Materials. He was awarded the Royal Microscopical Society's Glauert Medal in 1974 and is currently the Society's Vice President and International Secretary.

Malcolm Green was awarded his B.Sc. from the University of London in 1956 and his Ph.D. from Imperial College of Science and Technology, London, in 1959. From 1960–1963 he was an Assistant Lecturer in the Inorganic Chemistry Department at Cambridge. He moved to Oxford in 1963 on appointment as a Fellow in Inorganic Chemistry at Balliol College and was appointed University Lecturer in 1965. He was promoted to Professor of Inorganic Chemistry and head of the Inorganic Chemistry Laboratory in Oxford in 1988. He is a Fellow of the Royal Society, a Fellow of St Catherine's College, Oxford, and an Emeritus Fellow of Balliol College, Oxford.

DOI: 10.1039/b200537a

performed with respect to the inclusion of chemically functional or crystalline materials within such structures. As an example, Zhou *et al.* have shown that ruthenium cluster carbonyls form ordered arrays within the channels of mesoporous silica.[15] One would like to be able to study the templated encapsulated materials as discrete species and there are precedents for doing this. Where the host material can be dissolved or removed chemically from the inclusion material, then freestanding 1D structures will result. For example, it has been demonstrated that discrete Bi nanowires may be created from a porous alumina template following its chemical removal.[16] More recently Hong *et al.* have shown that 0.4 nm 1D silver wires can be extracted from the nanochannels of calix[4]hydroquinone *via* photochemical reduction of incorporated Ag^+ ions.[17] Studies of the physical properties of crystals formed on such a scale have been reported and, to this end, Kondo and co-workers have described the structure and quantum conductance behaviour of 1–2 atomic shell gold nanowires suspended between an STM tip and conducting substrate within a UHV High Resolution Transmission Electron Microscope (HRTEM).[18,19] This work showed that the conductance of a single strand of Au atoms equals $2e^2/h$ and that the conductance of a double shell of such atoms is twice as large.[18] These results provide clear motivation for more extensive and systematic studies into the formation and properties of atomically regulated low dimensional crystal structures, to wit 'Feynman Crystals'.†

Single walled carbon nanotubes (SWNTs)[20,21] are emerging as ideal model systems for studying discrete and atomically regulated crystal growth. These tubules, composed of rolled sheets of sp^2 graphene carbon terminated at one end by fullerenic carbon hemispheres, form well-defined cylindrical cavities (Fig. 1) within a strictly limited diameter range

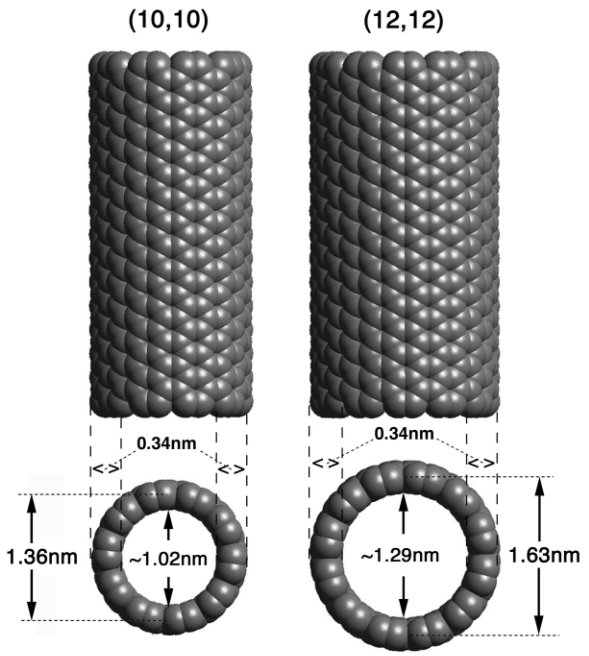

Fig. 1 Schematic representations of the van der Waals surfaces of (10,10) and (12,12) SWNTs with diameters of 1.4 and 1.6 nm and corresponding internal diameters of *ca.* 1.0 and 1.3 nm, respectively, as specified by the van der Waals radii of the sp^2 wall carbons.

(typically 1–2 nm) when prepared by either catalytic arc vapourisation[22] (*i.e.* Krätschmer–Huffman synthesis) or laser ablation.[23] Large quantities of such nanotubes can now be produced by a variety of catalyst-assisted decomposition techniques, most notably by pyrolysis of carbon monoxide in the presence of iron.[24] The effect of the size of these ultra-thin capillaries on the crystallisation of encapsulated molten binary species is to produce reduced or modified coordination structures. These deviations arise from the restriction of the guest material to as few as 2–3 atomic layers in cross-section, resulting in the formation of structures in which entire layers of coordinating ions have been excluded.[25,26] In other cases, the effect of capillary confinement is to produce reduced (relative to the bulk) coordination 1D-polyhedral chains or even structures with entirely novel coordinations and stereochemistry.[27–29]

The impact of this confining geometry on the low dimensional crystallisation properties of various halides with differing stoichiometries and bulk structure types and their subsequent characterisation is outlined in this review. We will demonstrate how atomically regulated Feynman Crystals are produced in SWNTs as a function of both the tubule diameter and the structural properties of the bulk material. We also describe modifications to these structures and recent developments in their characterisation.

Synthesis of 1D crystals within SWNTs

The first significant inclusions reported within SWNT capillaries were clusters and 1D nanowires of Ru metal [Fig. 2(a) and (b)].[30] The method of deposition used in this work involved immersing a sample of SWNTs, which had been pre-treated with concentrated HCl, in a saturated solution of $RuCl_3$. Following H_2 reduction, a low filling yield of 2–5% Ru metal was found inside the SWNT capillaries. The acidification step had been considered necessary in order to open the tips of the SWNTs which, at that time, were assumed to be closed by analogy with multi-wall carbon nanotubes (MWNTs).[31,32] Subsequently, it was shown that SWNTs could be filled without an opening step by capillary wetting[33,34] with molten mixtures of silver halides or mixtures of alkali and actinide halides [Fig. 2(c)].[35] Consequently, the now established capillary filling procedure consists of mixing the anhydrous halide with as-prepared SWNTs in a silica ampoule sealed under vacuum and then slowly heating the mixture to 50–100 K above the melting point of the respective halide followed by slow cooling. When the SWNTs were filled with silver halides, exposure to light was minimised.[35] By comparison with similar experiments performed with MWNTs, the ability of a molten material to wet and fill SWNTs depends on the criterion determined by Ebbesen for the filling of nanotubes with liquid phase media.[33,34,36] An interesting consequence of filling SWNTs with silver halides is the observation that, in tubules of greater than 2 nm in diameter, the halide undergoes spontaneous photolytic decomposition with the result that aligned 1D *fcc* silver nanowires are obtained within the capillaries [Fig. 2(d) and (e)].[35] A number of groups have now demonstrated that SWNTs can be filled with a variety of materials including metals and metal salts,[35–38] oxides,[39–41] helical iodine chains,[42] and 1D chains of fullerene[43–45] or endofullerene molecules.[46,47]

This review details our systematic study of the structural chemistry of a range of binary halide crystals [Table 1 and 2] encapsulated within SWNTs as these satisfy the wetting criterion described above and can be introduced by capillarity. In addition, we have extended the above synthetic methodology to mixed phase ternary systems[35,48] using a technique developed for the filling of pre-opened MWNTs with mixtures of KCl and UCl_4. This technique exploited the low temperature melting properties of the KCl–UCl_4 phase diagram in order to wet and fill MWNTs.[49] In the modified procedure, halide mixtures are ground together with as-prepared SWNTs and then heated to 50–100 K above the liquidus of the eutectic or thermal minimum temperature for the filling system employed [Fig. 3(a)–(c)]. In an improvement to the procedure, the halide mixtures were pre-melted in order to ensure compositional homogeneity for the filling media.[48] In cases where silver halide mixtures were used to fill SWNTs, exposure to light was again minimized and no pre-opening step was found to be necessary in these experiments.

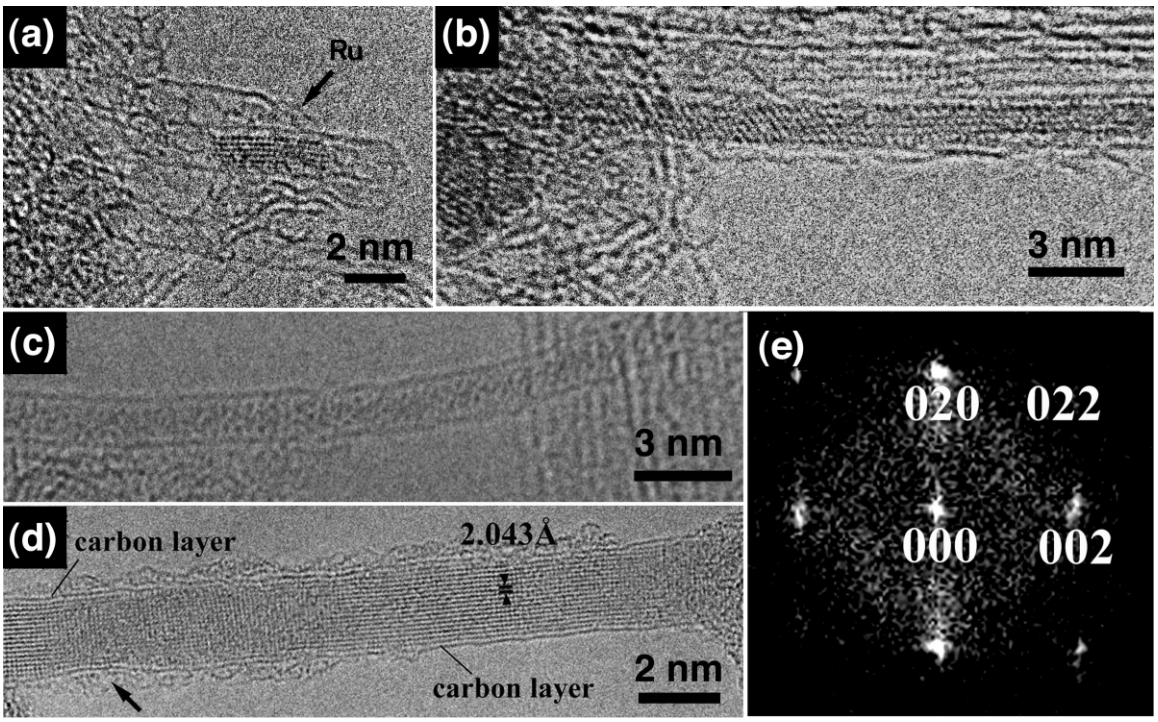

Fig. 2 (a) and (b) HRTEM images showing elongated Ru crystallites with aligned lattice fringes formed within SWNT capillaries. (c) HRTEM image showing the filling of an SWNT with a glassy mixture of KCl and UCl_4 [*i.e.* composition **B** in Fig. 3(a)]. (d) Image of a Ag 'nanowire' formed within a *ca.* 4 nm diameter SWNT. (e) Power spectrum, obtained from the arrowed region in (d) with reflections corresponding to Ag metal.

Table 1 General structure types of crystalline binary metal halides. The halides indicated in bold have all been encapsulated into SWNTs (adapted from ref. 53)

Stoichiometry	C.N.[a] of M	3D complex	C.N. of M	Layer	C.N. of M	Chain	C.N. of M	Molecular
MX	4	Zn blende	5 + 2	TlI (yel.)	2	AuI		
	6	**NaCl**, **AgX**[b]						
	8	**CsX**[b]						
MX_2	4	Silica-like	4	**HgI_2**	3	$SnCl_2$	2	$HgCl_2$
	4	ZnI_2		**(red)**	3	GeF_2		
	6	Rutile	6	**PbI_2**	4	$BeCl_2$	4	Pt_6Cl_{12}
	6	$CaCl_2$		**CdI_2**	4	$PdCl_2$		
	9	**SrI_2**, **BaI_2**, EuI_2		**$CdCl_2$**				
	7 + 2	$PbCl_2$						
	8	Fluorite	8	ThI_2				
MX_3	6	ReO_3-type	6	**$LnCl_3$**[d]	4	AuF_3	3	SbF_3
	7 + 2	LaF_3			6	ZrI_3	4	**Al_2Cl_6**
	8 + 1	YF_3	8 + 1	BiI_3			4	Au_2Cl_6
	9	UCl_3		$PuBr_3$				
		$LnCl_3$[c]						
MX_4	6	IrF_4	6	PbF_4	5	TeF_4	4	$SnBr_4$
	8	ZrF_4			6	α-NbI_4	4	**SnI_4**
	8	**UCl_4**, **$ThCl_4$**	8	ThI_4	6	**$ZrCl_4$**		
		TeI_4			6	**$HfCl_4$**		
MX_5	7	β-UF_5			6	BiF_5	5	$SbCl_5$
					6	CrF_5	6	Nb_2Cl_{10}
					7	$PaCl_5$	6	Mo_4F_{20}
MX_6							6	**WCl_6**
								IrF_6

[a] C.N. = coordination number. [b] X = Cl, Br and I. [c] Ln = La to Tb (UCl_3-type) only. [d] Ln = Tb ($PuBr_3$-type) to Lu only.

In addition to the incorporation of crystalline solid phase materials, a considerable amount of recent work has been devoted to the incorporation and study of molecular fullerenes[43–45] or endofullerenes[46,47] within SWNTs. The first fullerenes observed within SWNTs were 'naturally occurring' and were produced only in nanotubes formed by laser ablation[43] or arc vaporisation.[44,45] However, near-quantitative filling of SWNTs with fullerenes[50] or endofullerenes[51] is now possible *via* gas phase diffusion of fullerene molecules into heat-treated SWNT samples. It is interesting to note that in these experiments the SWNTs were either annealed *in vacuo* at up to 450 °C[50] or in dry air to 420 °C,[51] both of which result in high filling yields. Such experiments will help eliminate moisture or other capillary-absorbed species within the tubules thus improving the filling yield. Additionally, the direct incorporation of relatively inert fullerene molecules at just above their sublimation temperature[50,51] into SWNTs is a strong indication that the tubes are open at at least one end and the end caps therefore present no structural barrier to filling.

The self-organisation of fullerene molecules along SWNT capillaries also leads to one-dimensional crystals[47] in which the molecules are separated by approximately the van der Waals

Table 2 Packing behaviour observed in SWNTs as a function of bulk structure type

Halide filling	Common bulk structure type	C.N. in bulk	Structure inside SWNTs	C.N.s observed or predicted within SWNTs[a]
KI	3D rocksalt	6	Rocksalt	**4**,**5**,**6**
AgX[b]	3D rocksalt	6	Rocksalt	4,5,6
	Wurzite	4	Wurzite	**3**,**4**
CsX[b]	3D rocksalt	6	Rocksalt	4,5,6
	bcc	8	*bcc*[c]	4,6,8
SrI_2	3D network	7	1D PHC[d]	**4**,**6**
BaI_2	3D network	7 + 2	1D PHC[d]	**5**,**6**
UCl_4	3D network	8	1D PHC[d]	6,8
$ThCl_4$	3D network	8	1D PHC[d]	6,8
TeI_4	3D network	8	1D PHC[d]	6,8
LnX_3[d,e]	3D network	8 + 1	1D PHC[d]	6,8
HgI_2 (red)	2D layered	3	1D PHC[d]	2,3
PbI_2	2D layered	6	1D PHC[d]	**5**,**6**
CdI_2	2D layered	6	1D PHC[d]	5,6
$CdCl_2$	2D layered	6	1D PHC[d]	5,6
$LnCl_3$[d,f]	2D layered	6	1D PHC[d]	**5**,**6**
$ZrCl_4$	1D chain	6	1D PHC[d]	As bulk
$HfCl_4$	1D chain	6	1D PHC[d]	As bulk
Al_2Cl_6	Molecular	4	Packed molecular units	As bulk
SnI_4	Molecular	4	Packed molecular units	As bulk
WCl_6	Molecular	6	Packed molecular units	As bulk

[a] C.N.s in bold have been observed experimentally, the rest were predicted based on the observation of the microstructure of one strongly scattering sublattice. Bulk coordination is predicted for polyhedra in the centre of wide capillary SWNTs. [b] X includes Cl or Br and I. [c] Projected along <110>. [d] 1D PHC = 1D polyhedral chain. [e] Ln = La to Tb (UCl_3-type) only. [f] Ln = Tb ($PuBr_3$-type) to Lu only.

graphene separation (*ca.* 0.34 nm).[43] Recent electron diffraction measurements from bundles of SWNTs filled with different size and shape fullerenes have shown that these separations are in fact 3–4% smaller than those measured for bulk fullerene crystals.[52]

The formation and growth of atomically regulated KI crystals within SWNTs

For bulk halides, Wells has outlined a simple classification scheme according to stoichiometry, bulk structure type and coordination (Table 1)[53] which we have used as a guide for the filling of SWNTs.[54,55] In general, the effect of confining halides in SWNTs has been to form crystals in which, generally, the obtained structure is a function of (i) the bulk structure of the incorporated halide and (ii) the confining surface of the encapsulating nanotube. In a limited number of cases (i) does not hold and new structures result. The impact of confinement on the structural chemistry of the included halide crystals is summarised in Table 2. In this and in subsequent sections we outline the crystal packing properties of a representative group of halides within SWNTs of differing sizes and show how their structures may be distorted or otherwise modified by encapsulation.

For simple packed halides, confinement leads to the formation of 'Feynman Crystals' in which the number of atomic layers is precisely regulated. A first example is given by the formation of 'all-surface' 2 × 2 KI crystals within 1.4 nm diameter SWNTs [Fig. 4(a)–(c)].[25] The composite is imaged by conventional HRTEM as a 1D array of pairs of identical dark spots along the SWNT capillary. Each dark spot represents an I–K or K–I column viewed in projection as confirmed by comparison of lattice images with simulations [Fig. 4(d)–(f)]. This result is particularly significant as all the ions undergo a total reduction in coordination from 6:6 to 4:4. Lattice distortions were also observed in these 2 × 2 crystals. Measurements along the SWNT capillaries showed that the spots are spaced at average intervals of *ca.* 0.35 nm, corresponding to the {200} spacing of bulk KI, whereas across the SWNT capillary the spacing increased to *ca.* 0.4 nm, representing a *ca.* 14% tetragonal distortion.[25]

We have also reported the formation of a 3 × 3 KI crystal in a larger diameter (1.6 nm) SWNT [Fig. 5(a)–(c)].[26] In this case, the crystal was imaged along the cell diagonal (*i.e.* <110> relative to bulk KI) which has the advantage that, in this projection, it is possible to visualise the K^+ and I^- sublattices as pure element columns [Fig. 5(c)]. This, however, has presented some difficulties for conventional HRTEM imaging as it was not possible to observe the weaker scattering K^+ sublattice directly. However, using a modified through focal series restoration,[56] we have been able to restore the unaberrated phase [Fig. 5(a)] and modulus (not shown) of the exit surface wavefunction of the specimen.[26] Using this approach, the restored phase is obtained at close to the information limit of our HRTEM (*ca.* 0.1 nm) as opposed to the point resolution (*ca.* 1.6 nm) in conventional axial imaging. This additional information has made it possible to image the K^+ atom columns in addition to the more strongly scattering I^- atom columns [Fig. 5(a) and (b)]. Furthermore, the phase gives a more faithful representation of the projected electron density of the specimen which has enabled us to measure individual atom column displacements [Fig. 5(b)] within the incorporated 3 × 3 crystal (Table 3 in Fig. 5). This in turn has allowed us to construct a more detailed structural model [Fig. 5(c)] of the KI/SWNT composite than would have been possible *via* conventional HRTEM.

By analogy with the 2 × 2 KI crystal, the 3 × 3 crystal shows reduced surface coordination. In this case, three separate coordinations of 6:6, 5:5 and 4:4 are exhibited by the centre, face and corner …I–K–I–K… rows of the 3 × 3 crystal, respectively, along the SWNT axis.[26] In addition the iodine atoms located along <110> all showed a slight inwards compression relative to their positions in the bulk structure. The K atoms located along the same cell diagonal exhibited a small expansion and the K and I atoms located along the shorter <100> directions exhibited small expansions. We have attributed these distortions to the small compressive effect of the larger I^- ions (*i.e.* $I^-_{IV} \approx 0.22$ nm *vs.* $K^+_{IV} \approx 0.13$ nm) by the van der Waals surface of the SWNT.[55]

Computer simulations of 2 × 2 and 3 × 3 KI crystals in variable diameter SWNTs

Wilson and Madden have modelled the crystal growth behaviour of KI in variable diameter SWNTs using a molecular dynamics simulation approach.[57] The interactions between the ionic K^+ and I^- species were described by standard Born–

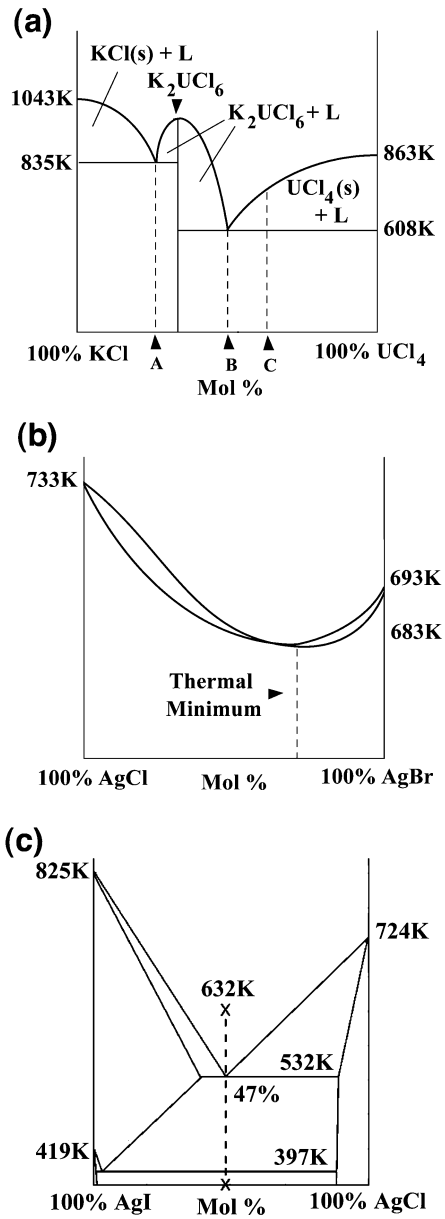

Fig. 3 Phase diagrams used to selectively fill SWNTs with ternary halide mixtures. (a) KCl–UCl_4 system: compositions **A**, **B** and **C** were used to fill SWNTs [see Fig. 2(c)]. (b) AgCl–AgBr system: the indicated thermal minimum was used to fill SWNTs. (c) AgCl–AgI system: the eutectic composition was used to fill SWNTs by first premelting the composition along the indicated temperature range and then heating the melt together with the homogenised eutectic along the same range (see also Figs. 11 and 12).

Mayer pair potentials with the assumption that the ions retained their formal integer charges. Interactions between the ions and the walls of nanotubes of varying diameters were described by Lennard–Jones potentials, with parameters derived from potentials for the interactions of isoelectronic inert gas atoms with the carbon atoms of an sp^2 graphene surface.

Time-resolved and minimum energy simulations (Fig. 6, Scheme **I**) predicted the filling of (10,10)[58] SWNTs with *thermodynamically ordered* arrays of 2 × 2 KI crystals starting from an open SWNT immersed in molten KI. Minimum energy simulations predicted lattice distortions that were consistent with those observed experimentally.[25] In the case of the 2 × 2 KI crystal, the correct aspect ratio for the observed lattice distortion of *ca.* 17% was obtained. In addition, for a 3 × 3 KI crystal encased in a 1.6 nm (12,12) SWNT, the differential displacements for halide atoms disposed along the longest < 110 > diagonal *versus* facial atoms disposed along the shorter < 100 > direction were reproduced. The extent of the distortions is given by the ratio $R = \boldsymbol{a}/\boldsymbol{b}$ (Fig. 6, Scheme **II** panels **A** and **C**). R is unity for the cubic bulk crystal but is distorted to 1.14 in the case of a 2 × 2 KI crystal inside a (10,10) SWNT encased in molten KI whereas $R = 0.84$ for a 3 × 3 KI crystal in an isolated SWNT although it decreases to 0.68 if the SWNT is surrounded by molten KI.[57] By comparison the experimental value of R is 0.8 for a K–2I–3K–2I–K layer and 0.92 for a I–2K–3I–2K–I layer as measured normal to the SWNT axis [Fig. 5(c)].[26]

1D crystals derived from polyhedral framework structures

In addition to the simple rocksalt-type structures described in the previous two sections, we have also introduced more complex 3D network, 2D layered, 1D chain and molecular halide structures into SWNTs (Table 1 and 2). By comparison with the 2 × 2 and 3 × 3 KI crystals, the structural chemistry of the crystals obtained within SWNTs can normally be described in terms of fragments derived from the corresponding bulk structures, albeit with local distortions of the anion and cation lattices in many instances. For most of these fragments, reduced coordinations are frequently predicted or inferred, as expected by analogy with those demonstrated for the KI fragments.[25,26] As with many bulk crystal structures, such as those indicated in Table 1, it is frequently more convenient to describe the encapsulated crystals in terms of coordination polyhedra although it follows that the crystals may just as easily be described in terms of simple sphere packing as for the encapsulated KI structures.

Fig. 7(a) shows an example of a 'twisted' $CdCl_2$ structure encapsulated within a SWNT.[54,59] Conventionally, $CdCl_2$ forms a structure (Table 1) that in the bulk consists of stacked 2D layers of edge-sharing $CdCl_6$ octahedra. In Fig. 7(b), a detail from the micrograph shows that either side of the twist, the microstructure of the crystal forms a 'zig-zag' array of dark spots within the SWNT capillary. This contrast is presumed to originate from the more strongly scattering Cd^{2+} ions rather than the weaker scattering Cl^- ions. We therefore attribute the 'zig-zag' contrast effect and the twisting behaviour to the formation of twisted 1D polyhedral chain of $CdCl_2$ [Fig. 7(c) and (d)]. The twisting phenomenon closely resembles that reported for helical iodine chains formed within SWNTs.[42] Fig. 7(e)–(h) illustrates the principle upon which this 'zig-zag' structure can be constructed in a 'top-down' fashion from the bulk crystal structure.[27,54] In this approach an appropriate 1D polyhedral chain is first selected from a single layer of the 2D parent structure [Fig. 7(e)]. If the bulk (*i.e.* octahedral) coordination is maintained within the 1D chain then a polyhedral chain with a stoichiometry of $CdCl_3$ results. However, if the Cl^- ions indicated in Fig. 7(g) are removed, then a polyhedral chain with the correct stoichiometry is produced [Fig. 7(h)]. Therefore, in this 1D nanostructure, the net coordination within the entire polyhedral chain is reduced from octahedral to square pyramidal.

A second example in Fig. 8 illustrates how a 1D crystal fragment of $TbCl_3$ can be formed from a more complex 3D polyhedral network structure.[28,55] In the HRTEM image [Fig. 8(a)], the structure appears as a 'zig-zag' array of dark spots formed in a peripheral nanotube within a SWNT bundle. In the enlargement [Fig. 8(b)] it is evident that groups of three spots define nearly equilateral triangles of side *ca.* 0.4 nm. This pattern corresponds to a 1D chain of $TbCl_x$ polyhedra [Fig. 8(c)] in which individual dark spots are due to the heavy Tb^{3+} centres. The bulk $TbCl_3$ structure [Fig. 8(d)] consists of a hexagonal network of edge-sharing 9-coordinate polyhedra. An intermediate model derived from this structure [Fig. 8(e)] with the same coordination is shown in Fig. 8(f). Owing to lattice termination, this 1D chain has a net stoichiometry of $TbCl_5$.

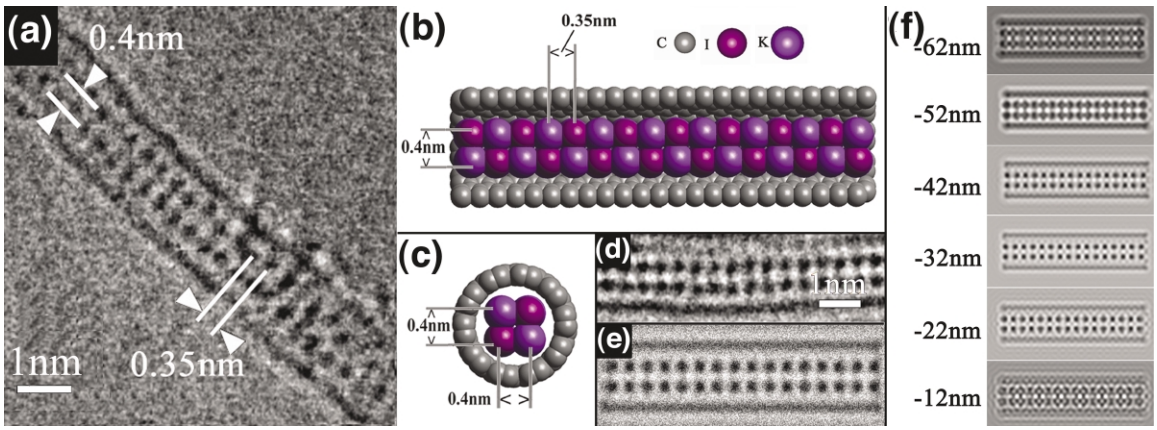

Fig. 4 (a) Conventional HRTEM image of a 2 × 2 KI crystal formed within a 1.4 nm diameter SWNT. (b) and (c) side-on and end-on structural representations of the 2 × 2 KI crystal within a (10,10) SWNT showing measured lattice distortions. (d)–(f) HRTEM image, calculated Scherzer focus image and calculated through focal series corresponding to (b) and (c).

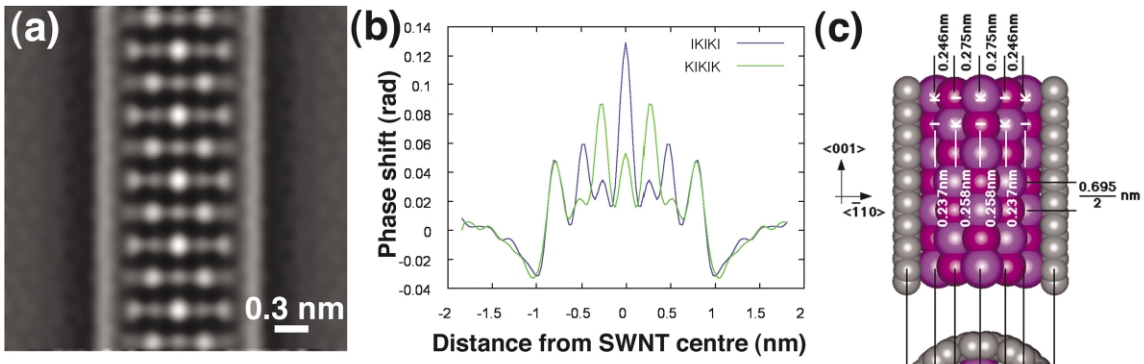

Table 3: distances of various atomic columns from the centre of the SWNT (nm).

layer	2K (2I)	1I (1K)	wall
IKIKI	0.258	0.495	0.79
KIKIK	0.275	0.521	0.79

Fig. 5 (a) Reconstructed phase (averaged along the tube axis) of the <110> projection of a 3 × 3 KI crystal in a 1.6 nm diameter SWNT. Note that the contrast in this image is reversed so that regions of high electron density appear bright and low electron density appear dark [*cf.* Fig. 4(a) and (d)]. (b) Plot derived from alternating I–2K–3I–2K–I and K–2I–3K–2I–K layers in (a) showing relative displacements of the atom columns (see Table 3). Outermost peaks are C layers; (c) structural model derived from (a).

However, if the three indicated Cl^- atoms in Fig. 8(f) are removed from each polyhedron, then the predicted structure [Fig. 8(g)] is obtained, corresponding to a 1D chain of 6-coordinate octahedra, with a correct stoichiometry of $TbCl_3$ [see Fig. 8(h)]. It is noteworthy that the derived chain has an identical structure to that of the 1D chain of $CdCl_6$ octahedra [Fig. 7(f)].

In a final example in Fig. 9, we show a 1D polyhedral chain of $ThCl_6$ units formed within a 1.1 nm diameter SWNT.[59] As for $CdCl_2$ and $TbCl_3$, the structure of the encapsulated material consists of a 1D 'zig-zag' array of dark spots with the image contrast being dominated by the strongly scattering Th^{4+} cations [Fig. 9(b)]. A 1D 'zig-zag' chain can be derived from the parent structure which consists of a 3D network of edge-sharing 8-coordinate polyhedra[60] to produced the composite structural model shown in Fig. 9(c). Fig. 9(d) shows a simulation of the effect of tilting this model through different angles with respect to the incident electron beam. When the polyhedral chain is viewed in a 'top down' projection (*i.e.* tilt angle = 0°) then the contrast due to the chain is visible as an unbroken straight line. However, as the composite is tilted through successively greater angles with respect to the incident beam, then the 'zig-zag' contrast becomes more and more pronounced until the chain is fully 'side-on' with respect to the electron beam (*i.e.* tilt angle = 90°). This simulation hence supports our interpretation of the 1D polyhedral chain structures.

With respect to the chain and molecular halides (Table 1), examples of these have been encapsulated within SWNTs as shown, in the first case, for $ZrCl_4$ (*vide infra*)[38] and for Al_2Cl_6, SnI_4 and WCl_6 (Table 1 and 2). As individual 1D chains or molecular units interact only with other like structural units through non-bonding type interactions, then we assume that these are incorporated into SWNTs with the same coordinations obtained in the bulk with one or more structural units forming within the nanotube capillaries. For 1D chain structures, the result will be a 1D polyhedral chain with the same coordination as the bulk and for molecular halides, the 1D obtained crystals will consist of packed molecular units held together by non-bonding interactions which also retain the same coordination as the bulk (Table 2).

A 1D BaI_2 chain with 5- and 6-coordination

BaI_2 is a further example of a 3D polyhedral framework binary halide structure which, in the bulk, forms three different variants according to the ambient pressure.[61–63] All of these structures can be described in terms of 3D networks of face-sharing coordination polyhedra exhibiting varying iodine

dispositions around a common tricapped trigonal prism motif [Fig. 10(a)–(c)]. Whereas the two lower pressure forms exhibit 9-coordination [Fig. 10(a) and (b); Table 1] the highest pressure version [Fig. 10(c)] exhibits 10-coordination. However, within the confines of a 1.6 nm diameter SWNT, this material was found to exhibit a completely different coordination scheme to that exhibited by any of these bulk forms.[29]

Fig. 10(d) and (e) show an image and corresponding detail of a BaI_2-filled SWNT. The microstructure of the filling material is clearly visible as a 2D array of dark spots which show a lower

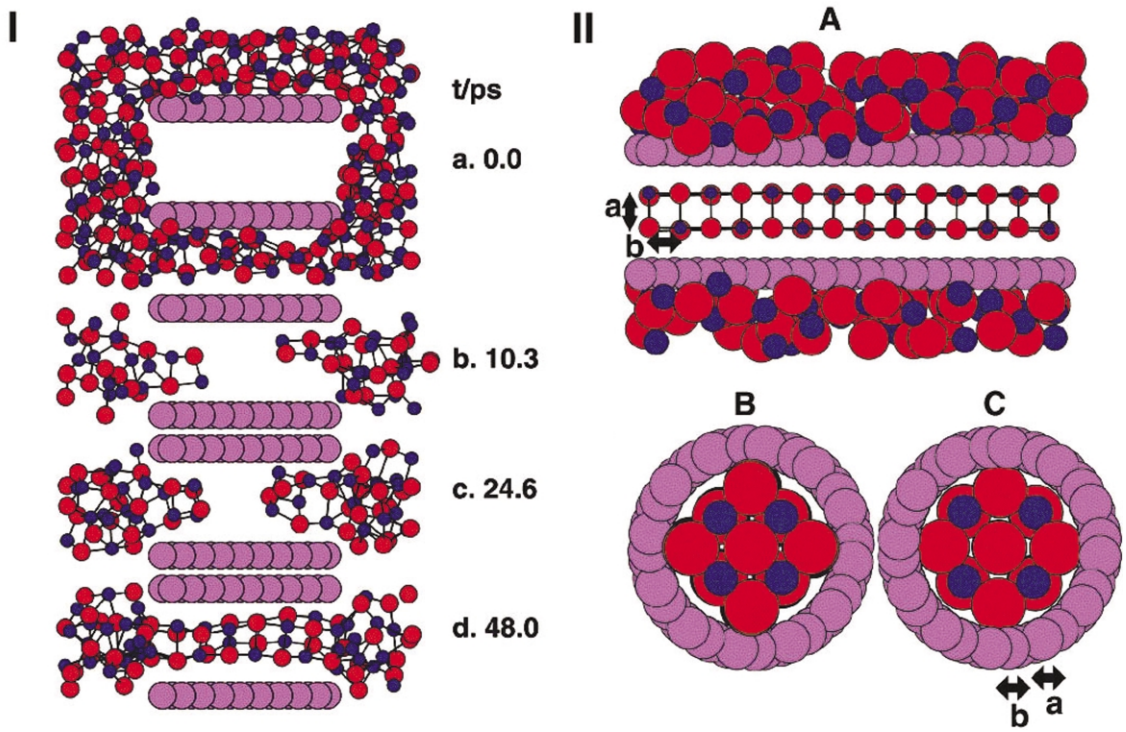

Fig. 6 Scheme **I**: time evolution study of an initially empty SWNT immersed in molten KI. Panel **a**: cross-section through initial configuration. Panels **b** and **c** show that KI only enters the tube when oppositely charged ions are paired and that substantial progress only occurs after the pairs have arranged as a 'finger' of the 2 × 2 crystal (external KI removed). The final configuration (panel **d**) shows the large amplitude vibrations (at 954 K) of the final embedded crystallite. Time averaging removes the disorder. Scheme **II**: minimum energy configurations obtained for KI under different conditions. Panel **A**: time averaged 2 × 2 KI crystal in a (10,10) SWNT. The lower panels show end-on views of a 3 × 3 KI crystal enclosed in an isolated (12,12) SWNT (panel **B**) and in a KI-encased (12,12) SWNT (panel **C**). Note the greater degree of deformation evident in the latter. (Schemes **I** and **II** adapted from ref. 55.)

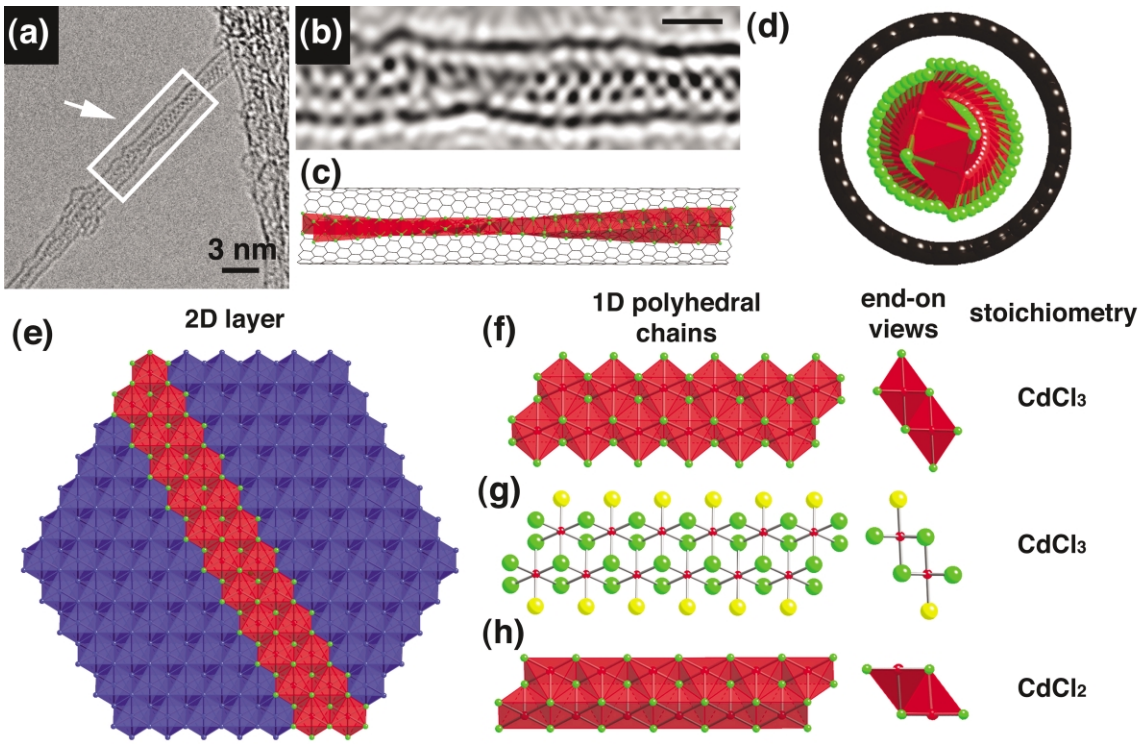

Fig. 7 (a) and (b) HRTEM micrograph and detail (scale bar = 1 nm) of encapsulated $CdCl_2$; (c) idealised representation of a twisted 1D polyhedral chain of $CdCl_2$ within a 1.1 nm chiral SWNT; (d) end-on view of (c); (e) single slice of a 2D $CdCl_2$ slab with a highlighted 'zig-zag' chain of $CdCl_6$ polyhedra; (f) discrete 1D chain of $CdCl_6$ polyhedra; (g) ball-and-stick representation of (f); (h) 1D chain of $CdCl_5$ square pyramids (correct stoichiometry).

intensity close to the walls of the SWNT and higher towards the centre. Since the electron scattering from Ba^{2+} is similar to that from I^- [*cf.* Ba (Z = 56) and I (Z = 53)] we propose that the dark spots correspond to 1–3 atom thick columns in projection, each of which may contain some combination of Ba^{2+} and I^- ions.

In order to construct a model for this crystal, a 2D peak mapping program was used to determine the relative positions of the atomic columns in Fig. 10(e), thus producing the atom map reproduced in Fig. 10(f). In order to complete the crystal, this planar fragment was expanded vertically to give the end-on representation shown on the right of Fig. 10(f) in which the

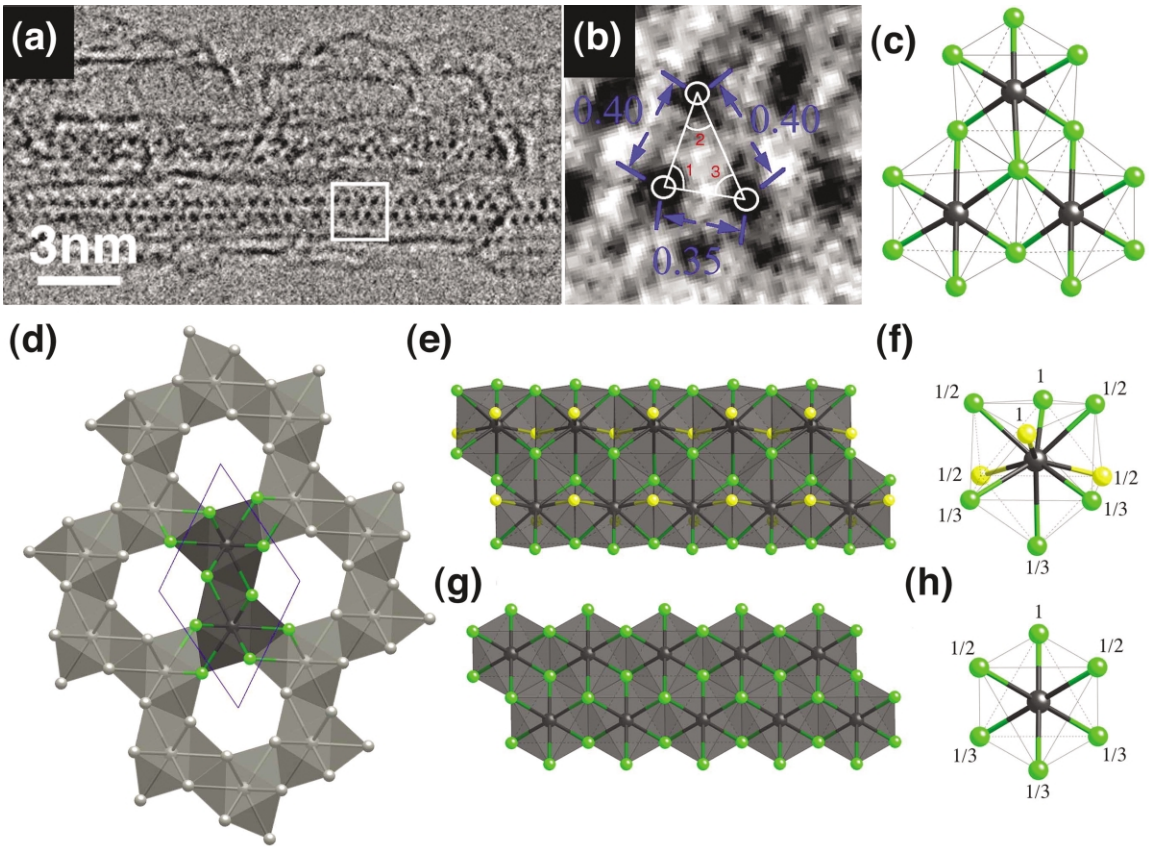

Fig. 8 (a) and (b) HRTEM micrograph and enlargement of a 1D polyhedral chain of $TbCl_3$ formed in the peripheral SWNT; (c) schematic representation of three $TbCl_6$ polyhedra; (d) bulk hexagonal $P6_3/m$ $TbCl_3$ structure with highlighted polyhedral chain; (e) 1D chain of $TbCl_9$ of 9-coordinate polyhedra derived from (d) (*i.e.* rotated 90°); (f) coordination and anion sharing model for polyhedra in (e); (g) 1D chain with $CdCl_2$-type structure formed by removal of excess terminating chlorines (indicated in yellow) in (f); (h) final coordination and anion sharing predicted for a single $TbCl_6$ polyhedron in the 1D chain in (g).

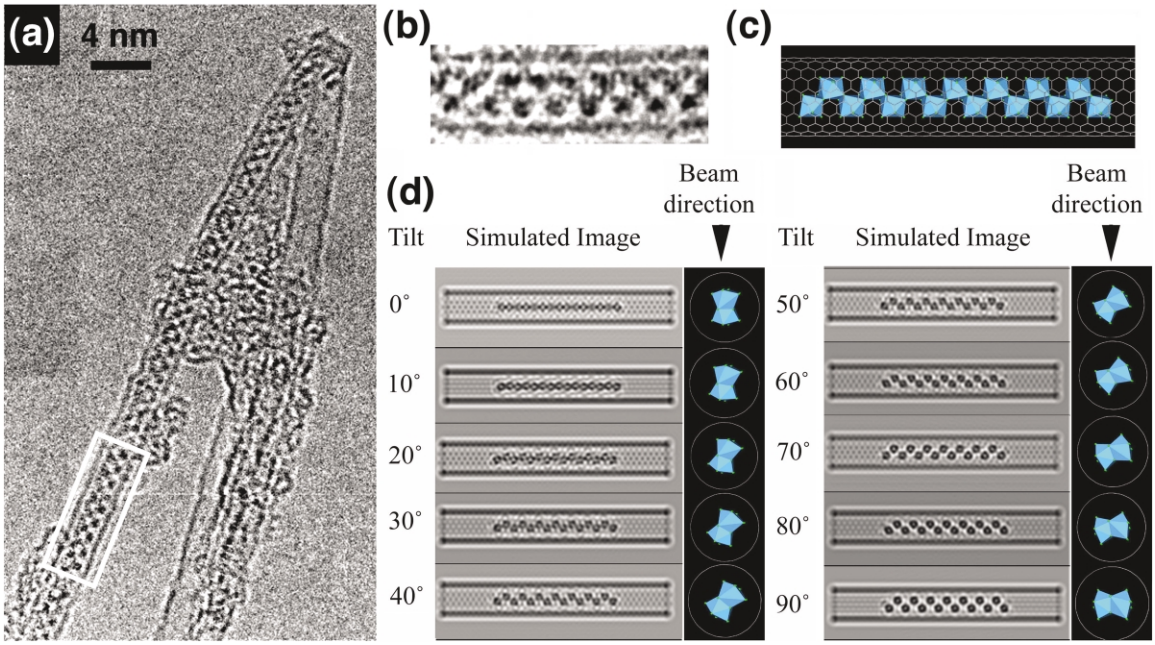

Fig. 9 (a) HRTEM image of a 1D $ThCl_6$ chain formed within a bent 1.1 nm diameter SWNT; (b) detail from boxed region in (a); (c) predicted composite structural model; (d) series of simulations calculated for the Scherzer defocus showing the effect of tilting the 1D composite at various angles with respect to the incident electron beam.

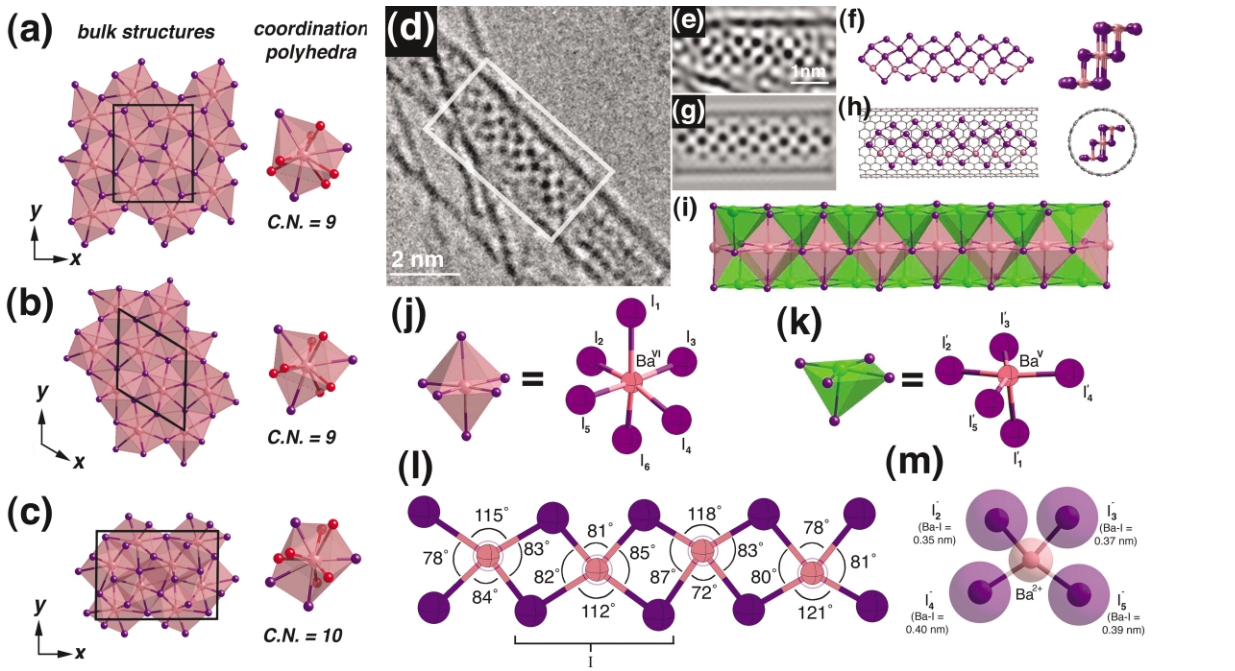

Fig. 10 (a) Nine-coordinate cotunnite *Pnam* form of BaI_2 formed under ambient conditions; (b) 9-coordinate hexagonal $P\bar{6}2m$ modification of BaI_2 formed under 3 GPa pressure; (c) 10-coordinate $P112_1/a$ form of BaI_2 formed between 5 and 15 GPa pressure; (d) and (e) HRTEM image and detail of a 1D BaI_2 chain formed within a SWNT; (f) side-on and end-on views of the atom positions derived from the lattice image; (g) Scherzer focus simulation of derived composite; (h) side-on and end-on views of the composite; (i) coordination model derived for a 1D BaI_2 chain; (j) and (k) 6- and 5-coordination polyhedra observed within the 1D chain; (l) measured equatorial bond angles within the central region of the BaI_2 1D chain; (m) representative equatorial bond distances for I in (l).

fragment may be considered as being 1–2–3–2–1 atomic layers in thickness. Atomic positions were assigned based on a coordination scheme for Ba and I that would retain Ba in a +2 oxidation state. The vertical expansion was scaled according to the Ba–I bond distance anticipated from the ionic radii of Ba_{VI}^{2+} (0.136 nm) and I_{VI}^{-} (0.22 nm). A simulated HRTEM image [Fig. 10(g)] calculated from this composite crystal and consisting of a section of a (12,12) SWNT and the derived crystal fragment [Fig. 10(h)] provides good agreement with the experimental image. The coordination polyhedra model derived from this 1D chain [Fig. 10(i)] results in octahedral coordination for the Ba^{2+} ions along the centre of the chain [Fig. 10(j)] and pentagonal coordination for the Ba^{2+} ions on the edges of the chain [Fig. 10(k)].

It was also possible to derive information about some of the I–Ba–I bond angles and distances within the 1D chain. Equatorial I–Ba bond angles were estimated from the spot dispositions in the lattice image [Fig. 10(l)]. Apical Ba–I distances were estimated from the ionic radii of Ba^{2+} and I^{-} (see above) while equatorial I–Ba distances were estimated from intercolumnar distances measured from the dark spots giving values ranging from 0.35 to 0.40 nm. The estimated Ba–I distances were found to be either equal to or higher than Ba–I distances predicted from the ionic radii. The resultant anion and cation dispositions in the BaI_2 chain were found to be completely different from any of those reported for barium iodide structures[61–63] and we therefore conclude that the 1D BaI_2 chain exhibits an entirely novel structure within SWNTs.

Halide cluster formation within SWNTs

Following extended exposure to an intense electron beam, 1D chains of halide crystals formed within SWNTs segregate into discrete clusters.[38] $ZrCl_4$ which itself is a chain-type halide structure (Table 1) readily intercalates into SWNTs presumably to form unreduced 1D polyhedral chains within their capillaries. Irradiation of this composite with a high intensity electron beam caused the filling material to undergo progressive changes in morphology as it segregates to form clusters. These decomposition events were observed to take place more rapidly than the denaturing of the SWNTs which eventually becomes catastrophic once such tubules are irradiated for periods of more than a few minutes at intermediate accelerating voltages.[64,65]

The decomposition of $ZrCl_4$ was observed *in situ* within a Field Emission Gun HRTEM (FEGTEM) using a beam current density of *ca.* 5×10^5 e^- nm^{-2} s^{-1}, equivalent to a current of *ca.* 2.7×10^{-14} A.[38] Fig. 11(a) shows a typical sequence of images obtained over a period of *ca.* 4 min. In the initial image (**I**), two continuously filled SWNTs can be seen with the upper tubule terminated by a cap visible on the right of the image. By image **II**, the filling in the bottom tubule had already segregated into three *ca.* 3–4 nm long clusters. Subsequently in image **V** the arrowed clusters were found to have different lengths of 3, 2 and 4 nm. In image **VI**, the material in the topmost tubule had also segregated into two clusters. The final image (**X**) shows discrete *ca.* 1 nm long clusters in the two nanotubes with the number of clusters in the bottom tubule increasing from three (*cf.* image **V**) to four. It is important to note that during these initial transformations, the walls of the tubules appeared to be unchanged, indicating that no chemical interaction between the carbon walls and the filling material had occurred during clusterisation. In addition, a minimum length of *ca.* 1 nm for the clusters was eventually obtained after irradiation for *ca.* 10 min. The microstructure of the filling material in image **I** is indistinct whereas several of the longer clusters in images **II**, **III** and **V** consist of 1D arrays of dark spots similar to those described for $CdCl_2$ and other similar structures.[27,28,54,55,59] It is therefore reasonable to suppose that $ZrCl_4$, which forms an edge-sharing 'trans' octahedral chain structure in the bulk,[66] forms similar 1D chains within SWNT capillaries. Electron beam bombardment of MX_n halides at intermediate accelerating voltages (typically 100–400 kV) produces isolated, stoichiometric, Frenkel-type defects in bulk crystals.[67,68] However, in smaller volume halide crystallites (*ca.* 1 μm^3 particle size) elimination of halogen and formation of surface metal occurs instead.[69] We have proposed therefore that the 1D $ZrCl_4$ chains undergo sequential elimination of chlorine to form clusters of $ZrCl_x$, of progressively lower

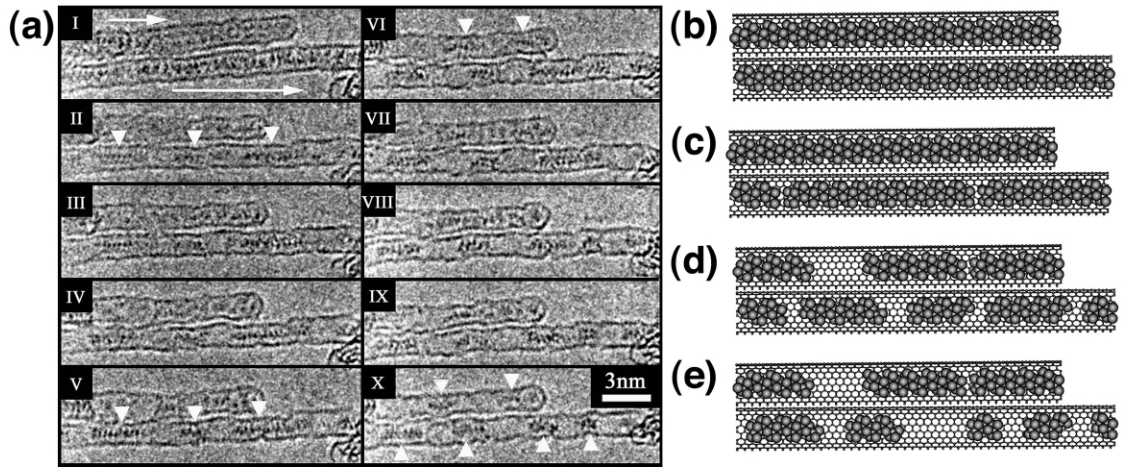

Fig. 11 (a) Sequence of images **I** to **X** obtained at *ca.* 20 s intervals showing gradual clusterisation of $ZrCl_4$ induced by e^-beam irradiation; (b)–(e) idealised structural representation of cluster formation within a pair of SWNTs.

stoichiometry (*i.e.* $\times$ decreases from 4 to 0), according to the idealised schematic representation in Fig. 11(b)–(e). Initially [Fig. 11(b)], the continuous filling of an unbroken $ZrCl_4$ chain is shown. Partial irradiation causes breaks in the chain [Fig. 11(c)] and, at the sites of these breaks, elimination of Cl_2 occurs resulting in the formation of reduced polyhedra at the chain termini. It has been assumed that molecules of Cl_2 diffuse out of side-wall defects or the end-caps of the SWNTs. During further irradiation, smaller clusters form [Fig. 11(d)] followed by discrete, separated clusters [Fig. 11(e)]. While electron beam-induced coalescence of fullerene and endofullerene molecules has been reported within SWNTs,[43,44,67] this was the first time that cluster segregation of a solid phase material was reported. If this mode of cluster formation can be reproduced for a bulk semiconductor-filled SWNT sample – for example, by use of an alternative decomposition methodology – then it will be possible to produce aligned 1D quantum dot arrays within SWNTs.

Imaging and electron energy loss spectroscopy of a 1D metastable ternary halide structure

In addition to the binary halide structures described above, we have been successful in incorporating ternary halide mixtures into SWNTs using the mixed halide approach outlined earlier.[35] The formation of crystalline ternary halides within SWNTs must be seen as an important 'next step' in terms of composite synthesis as it will enable further chemical tuning of the inclusion crystals. However, characterisation of inclusions containing more than two elements has proven to be difficult and, until recently, we were unable to provide information concerning their local crystallinity or composition. In this section we outline how HRTEM and spatially resolved Electron Energy Loss Spectroscopy (EELS), previously applied to the characterisation of oxide and endohedral fullerene SWNT inclusions,[39,47,51,70] may be used for the systematic characterisation of a metastable ternary crystalline inclusion phase.

Using the melting properties of the pseudoternary AgCl–AgI phase diagram [Fig. 3(c)], we incorporated the eutectic AgCl–AgI composition into SWNTs using the procedure outlined earlier.[35,48] This composition was chosen as is contains one strongly scattering halogen [*i.e.* I (Z = 53) *vs.* Cl (Z = 17)] which should facilitate preferential imaging *via* HRTEM and also *Z*-contrast imaging in Scanning Transmission Electron Microscopy (STEM) has been used in the direct imaging of helical iodine chains formed within SWNTs.[42]

HRTEM performed on the composites formed between SWNTs and the AgCl–AgI mixture revealed that the tubules contained a mixture of filling materials. Approximately 70% of the observed filling was crystalline, although *ca.* 30% was disordered. The crystalline filling consisted of: (i) a metallic Ag filling as shown in Fig. 12(a)–(c), presumed to originate from dissociation of the halide mixture as described in an earlier section for the AgCl–AgBr filling;[35] and (ii) crystalline $AgCl_{1-x}I_x$ filling [Fig. 12(d) and (e)]. The latter was found to be metastable as the AgCl–AgI eutectic composition is polycrystalline in the solid state.

Fig. 12(a) shows a *ca.* 2 nm diameter SWNT filled with the *fcc* Ag metal with $<010>$ parallel to the SWNT axis and $<001>$ parallel to the electron beam. Measurements from the image and corresponding power spectrum [Fig. 12(b)] gave an average lattice spacing orthogonal to the SWNT axis of *ca.* 0.21 nm, corresponding to d_{020} for bulk Ag. The walls of the encapsulating tubule are visible as vertical lines either side of the Ag nanocrystal, which comprises eight {200} layers arranged parallel to the SWNT axis [Fig. 12(c)]. Fig. 12(d)–(f) shows a HRTEM image, enlargement and corresponding power spectrum of the crystalline halide filling formed in a 1.4 nm diameter SWNT. An average periodicity of *ca.* 0.4 nm was established along the SWNT axis. An enlargement [Fig. 12(e)] reveals that the microstructure consists of a staggered array of distorted dark spots. The lattice spacing and spot configuration suggest a 1D 'tunnel' structure derived from wurzite AgI [Fig. 12(g) and (h)]. Bulk wurzite AgI consists of stacked hexagonal double layers of tetrahedrally coordinated Ag and I separated by *ca.* 0.37nm (*i.e.* d_{002}). Therefore, according to our model, each dark spot in the lattice image corresponds to slightly staggered X–Ag–X or Ag–X–Ag columns [bottom of Fig. 12(g)]. Fig. 12(e) indicates that the dark spots show unsystematic contrast variations which are attributed to a random distribution of weaker scattering Cl and stronger scattering I over the X sites [Fig. 12(g) and (h)]. It is particularly noteworthy that the formation of such a structure would be accompanied by a reduction in coordination for Ag from tetrahedral to trigonal, which may account for the expansion of d_{002} to 0.40 nm. This bears a close resemblance to the distortions for the other structural families described in previous sections.

EELS line scans were used to probe the local compositions of this nanocomposite. Fig. 12(i) shows a typical High Angle Annular Dark Field (HAADF) STEM image obtained from a SWNT bundle. Fig. 12(j) shows an end-on view of a 3D plot of 26 spectra obtained along the indicated line **I**–**II** in Fig. 12(i). The height of the dominant C–K absorption edge gives an indication of the thickness of the bundle with respect to probe position. A representative EELS spectrum with resolved Cl–$L_{2,3}$, Ag–$M_{4,5}$ and I–$M_{4,5}$ edges is shown in Fig. 12(k). The I and Cl edges were always observed together whenever halide was detected, indicating that the AgCl–AgI mixture melted congruently into the SWNTs. In addition Cl : I ratios measured from counts obtained from multiple background subtracted and

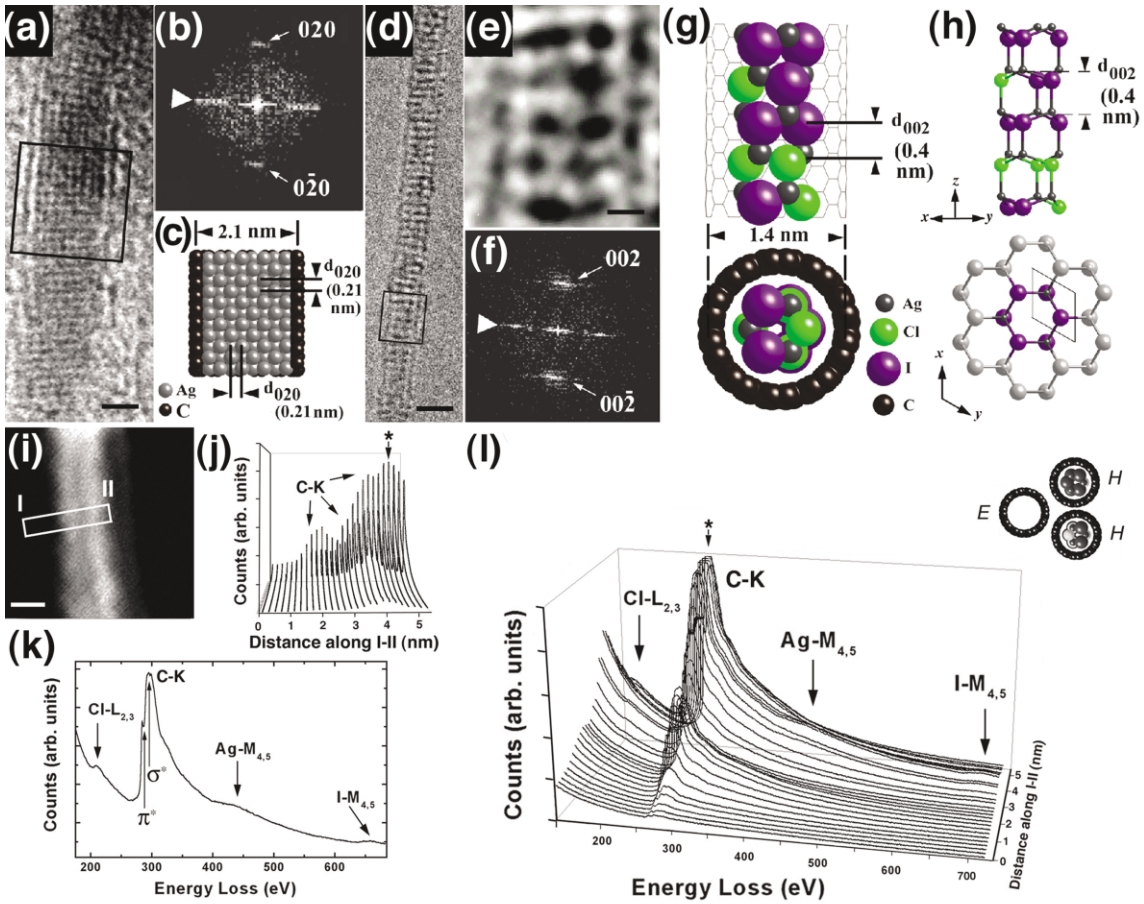

Fig. 12 (a) HRTEM image of Ag crystal within a SWNT (scale bar = 1 nm); (b) power spectrum from (a); (c) structure model; (d) and (e) HRTEM image (scale bar = 2 nm) and detail (scale bar = 0.2 nm) of crystalline $AgCl_{1-x}I_x$; (f) power spectrum from (d); (g) side-on (top) and end-on (bottom) representations of 1D wurzite tunnel structure; (h) staggered ball-and-stick representation (top) and schematic showing derivation (bottom) of tunnel structure from < 001 > of wurzite AgI; (i) HAADF image showing partially filled SWNT bundle (scale bar = 2 nm); (j) end-on view of a 3D plot of EELS spectra obtained along **I** to **II** ; (k) representative EELS spectrum; (l) perspective view of 3D EELS plot (inset: predicted filling configuration; key: E = empty SWNT; H = halide-filled SWNT); the asterix indicates the individual spectrum shown in (k).

integrated Cl and I absorption edges varied from *ca.* 10 : 1 to 1 : 10, thus supporting the observation that local concentrations of Cl and I vary on an unsystematic basis. The perspective view of the 3D plot [Fig. 12(l)] shows the evolution of the EELS spectra along **I**–**II**. The Cl, Ag and I edges are absent from the group of peaks corresponding to the SWNT nearest to **I**, indicating that this tube is empty.

In Fig. 13 pre-scan and post-scan HAADF images, corresponding contrast profiles, predicted filling configurations and integrated EELS linescan profiles, from four different $AgCl_{1-x}I_x$-filled SWNT bundles [(i)–(iv)] are presented. In the case of the EELS profiles, the counts corresponding to the C–K, Cl–$L_{2,3}$, Ag–$M_{4,5}$ and the I–$M_{4,5}$ edges have been background subtracted and integrated in order to provide spatially resolved concentrations for all four elements in each spectrum. The HAADF image and contrast profile for (i) shows a clearly defined pair of SWNTs and the EELS profile shows that both contain all three elements conforming to $AgCl_{1-x}I_x$. The small depression in the middle of the four EELS profiles corresponds to the gap between the two SWNTs visible in the HAADF image. The EELS profile for (ii) indicates that SWNT bundle in the HAADF image contains *ca.* five SWNTs in a 2:2:1 configuration with only the central two SWNTs containing halide filling. The contrast profile and HAADF image for (iii) indicates that the SWNT bundle contains *ca.* four SWNTs in a 1:2:1 configuration. The EELS profile corresponding to the outermost SWNT (*i.e.* closest to **I**) contains Ag only, indicating that this tubule contains a decomposed nanowire of Ag metal whilst the profile from the centre of the bundle indicated that all three elements are present. The outermost tube on the right hand side (closest to **II**) may also contain pure Ag. Fig. 13(iv) shows results from a larger bundle of SWNTs with a 2:3:2:2:2 configuration, based on the C–K profile. In this case the thick group of tubules nearest to **I** are clearly empty whereas the centremost and peripheral tubules closest to **II** contain significant filling. The post-scan HAADF images on the right of Fig. 13 indicate that the EELS probe caused considerable damage to the SWNT samples. While this did not affect our ability to obtain EELS spectra, it indicates that the samples underwent considerable rearrangement during linescan acquisition.

Molecules meet crystals: simultaneous observation of 1D crystals and fullerenes within SWNTs

As has been described previously, both fullerene molecules and endofullerene molecules containing one or more elements may be incorporated within SWNTs.[43–47,50–52,67] The size of the molecules that can be formed within SWNTs are found to be influenced by the diameter of the encapsulating nanotubes, a result which parallels our observation that the diameter of the SWNTs regulates the number of atomic layers formed within a 1D crystal encapsulated within a SWNT.[25,26] Indeed, the first naturally occurring fullerenes observed within a 1.4 nm diameter SWNT found in a sample synthesised by laser ablation were predominantly C_{60} molecules 0.7 nm in diameter although other fullerenes were also present.[43] Image simulations conclusively demonstrated that larger fullerene molecules, possibly corresponding to C_{80}–C_{84} could be incorporated within 1.5 nm SWNTs [Fig. 14(a)].[44] A systematic study of fullerene diameter

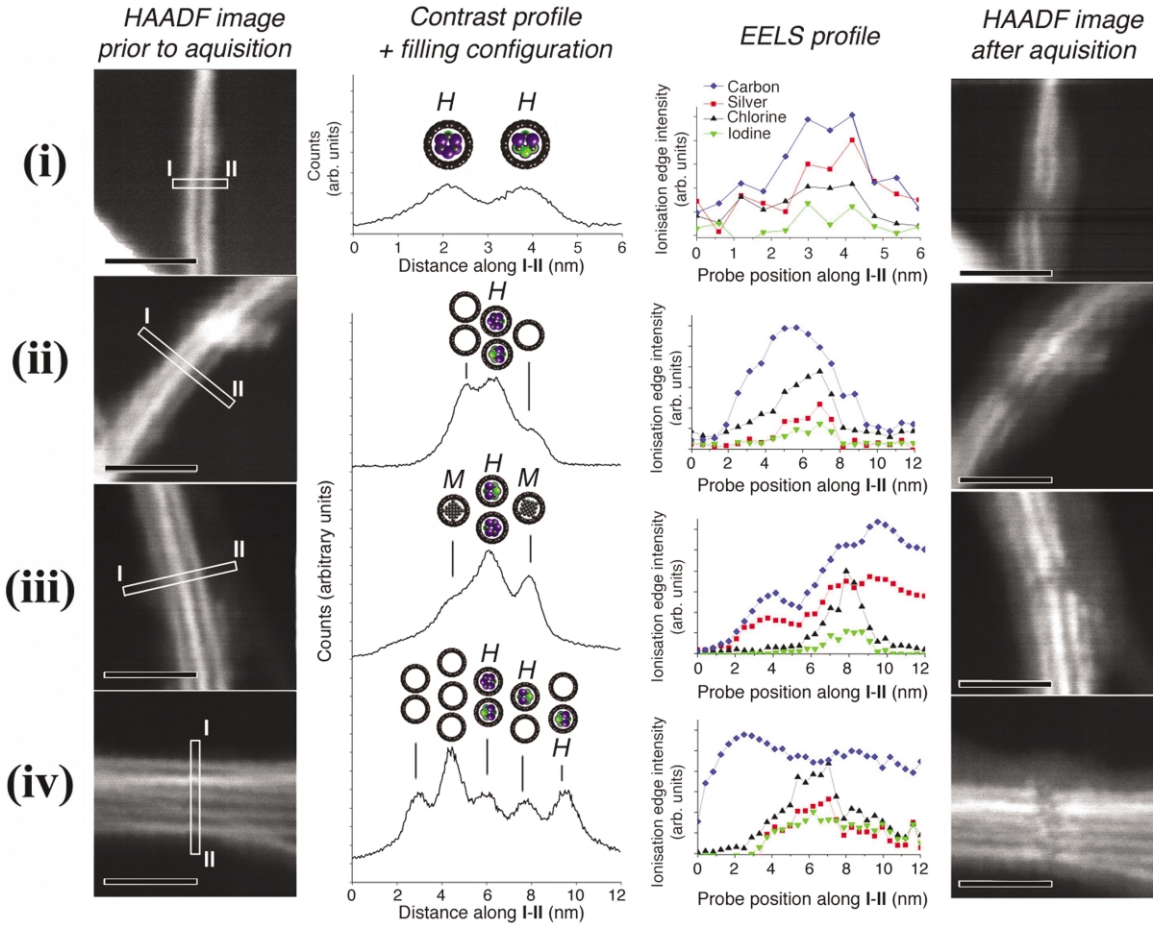

Fig. 13 Left to right: pre-EELS HAADF images, contrast profiles and filling configurations (key: *H* = halide-filled SWNT; *M* = metal-filled SWNT), integrated EELS profiles and post-EELS HAADF images obtained from (i) a pair of SWNTs; (ii) and (iii) two bundles containing *ca.* four SWNTs; and (iv) a bundle containing 8–9 SWNTs, respectively (all scale bars = 10 nm).

versus encapsulating tubule diameter [Fig. 14(b)] clearly demonstrated that the size distribution of the obtained encapsulated fullerenes is controlled by the diameter of the encapsulating nanotube.[44]

As fullerenes are formed within as-prepared SWNTs,[43–45] there exists the possibility that these could obstruct 1D crystal growth. In fact, we have been able to observe the blockage of SWNT capillaries by fullerene molecules and, as a result, have been able to study directly fullerene:1D crystal interfaces as shown in Fig. 15.[44,59,71] In Fig. 15(a) and (b), a HRTEM image and idealised structural representation of a mixed fullerene:$ThCl_4$ interface are shown. The fullerenes exhibit variable

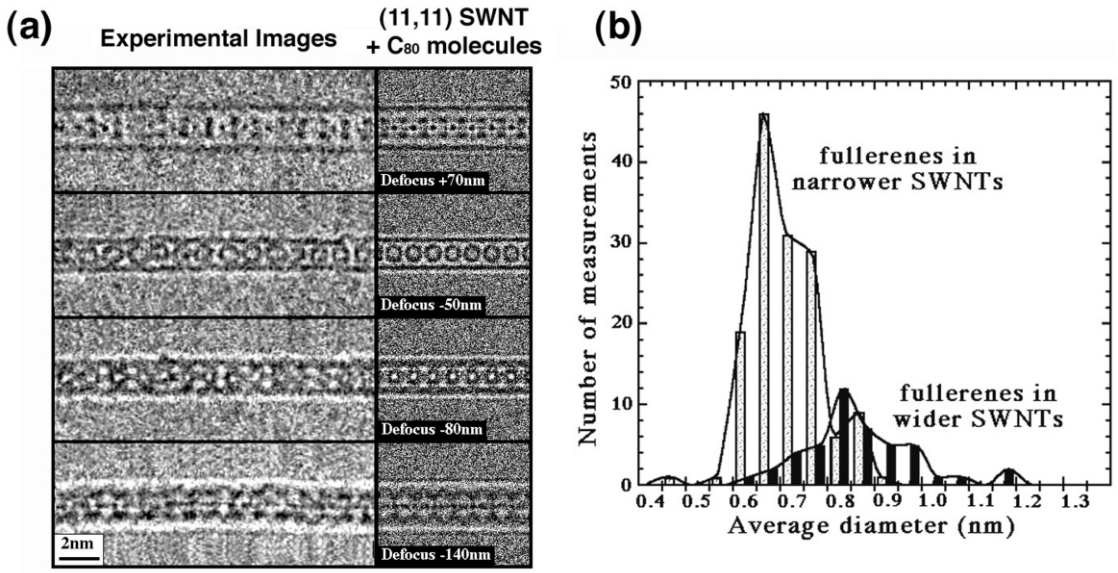

Fig. 14 (a) Experimental through focal series of HRTEM images of a SWNT filled with 14 fullerene molecules (left column). The right hand column shows image simulations with added random noise calculated for a (11,11) SWNT incorporating a chain of C_{80} molecules; (b) measured fullerene diameters in SWNTs of 1.35–1.40 nm diameters (light shading) and 1.55–1.60 nm diameters (dark shading).

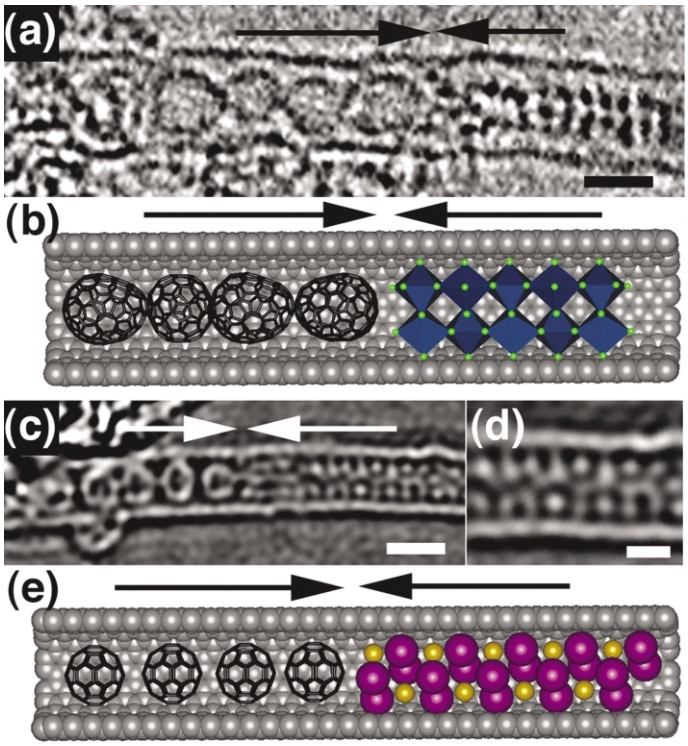

Fig. 15 (a) HRTEM image showing an interface within a SWNT formed between four different size and shape fullerene molecules and a 1D $ThCl_4$ crystal (scale bar = 1 nm); (b) schematic structure representation of (a); (c) and (d) restored phase (scale bar = 1.5 nm) and detail (scale bar = 1 nm) showing an interface between four fullerene molecules (a possible fifth molecule is obscured at the left) and a 1D FeI_2 crystal; (e) schematic structure representation of (c) (Fe atoms = light brown spheres; I atoms = purple spheres).

diameters, in accordance with the observations above. Surprisingly the $ThCl_4$ structure does not exhibit the 'zig-zag' structure illustrated in Fig. 8 but instead consists of a double layer of dark spots which we believe results from the formation of two, stacked, 'zig-zag' chains viewed in projection as illustrated in Fig. 15(b). In Fig. 15(c) and (d) a restored phase image and detail obtained from a fullerene–FeI_2–SWNT composite are shown. On the left of Fig. 15(a), four 0.7 nm diameter fullerenes are observed while on the right, a complex contrast corresponding to the FeI_2 1D crystal can be seen. This latter contrast consists of a 'zig-zag' array of white spots interspersed with white lines as shown in the detail [Fig. 15(d)]. We believe that the white spots originate from discrete Fe columns (possibly containing one or more iodine atoms) and that the lines originate from the coordinating I atoms in which the atom columns are staggered [Fig. 15(e)].

It would be an interesting exercise to observe the filling with a liquid phase material of a fullerene-blocked SWNT *in situ* and in real time. Given the chemical similarity between fullerenes[72] and SWNT end caps[20,21] it would be interesting to observe whether the advancing filling material attacked some of the fullerene molecules, comes to a dead stop against them, or simply pushes them along the capillaries. These observations may at least help to clear up the issue of as to whether or not molten media attack the fullerenic end caps chemically.[35]

Conclusions

In this paper we have reviewed experimental evidence for templating and modification of a variety of different types of 1D halide crystals within SWNTs. Within these very narrow capillaries the structures obtained are frequently found to be an integral number of atomic layers in two dimensions and are effectively infinite in the third. As a result, precise and atomically regulated or 1D Feynman Crystal growth is possible. The form of the structures varies depending on whether the bulk material is a simple packed structure (*e.g.* rocksalt or wurzite) or whether it can be described more readily in terms of 1D chains of simple coordination polyhedra. Occasionally, unique structures unrelated to the bulk halides are formed as a result of encapsulation. The structures nearly always exhibit reduced coordination as a result of lattice terminations enforced by capillary confinement. It is possible to modify the inserted crystals chemically either by photolytic reduction, or by *in situ* e^--beam irradiation experiments with the result, in the latter case, that 1D crystals may be reduced to form metallic wires or templated 0D nanocrystals of strictly regulated sizes. Fundamentally, the ability to control materials formation precisely can be realised by SWNT encapsulation and a key part of Feynman's vision therefore demonstrated.

Acknowledgements

The authors are indebted to a large number of collaborators who have contributed to this project, including, in Oxford: Marek Zweifka-Sibley, David Wright, Gareth Brown, Sam Bailey, Steffi Friedrichs, Cigang Xu, Miles Novotny, Neal Hanson, Sara Grosvenor, Eilidh Philp, Dr Jens Hammer, Dr Karl Coleman, Dr Cliff Williams, Professor Hee-Gweon Woo, Dr Emmanuel Flahaut, Dr Rafal Dunin-Borkowski and, in Cambridge: Rüdiger Meyer and Dr Owen Saxton. We are also grateful to contributions from Dr Mauricio Terrones (currently at IPICyT, Mexico), Dr Stefan Nufer and Professor Manfred Rühle of the Max Planck Institut für Metallforschung, Stuttgart, and from Dr Mark Wilson and Professor Paul Madden FRS of the Physical and Theoretical Laboratory, Oxford. We acknowledge financial support from the Petroleum Research Fund, administered by the ACS (Grant No. 33765-AC5) and the EPSRC (Grant Nos. GR/L59238 and GR/L22324). J. S. is indebted to the Royal Society for a University Research Fellowship.

Notes and references

† For the purposes of this article, a Feynman Crystal is defined as any crystal structure in which the number of atomic layers is regulated in a

strictly integral fashion (*i.e.* 1,2,3…*etc.* atomic layers) in one or more dimensions. A 2D Feynman Crystal is thus constrained in one dimension, a 1D Feynman Crystal is constrained in two dimensions and a 0D Feynman Crystal is therefore a single atom.

1 Reproduced in R. P. Feynman, *Eng. Sci.*, 1960, **23**, 22; see also: http://www.zyvex.com/nanotech/feynman.html.
2 D. Bimberg, M. Grundmann and N. N. Ledentsov, *Quantum Dot Heterostructures*, John Wiley & Sons Ltd., Chichester, 1999.
3 R. M. Overney, E. Meyer, J. Frommer, D. Brodbeck, R. Luthi, L. Howald, H.-J. Guntherodt, M. Fujihira, H. Takano and Y. Gotoh, *Nature*, 1992, **359**, 133.
4 A. Noy, C. D. Frisbie, L. F. Rozsnyai, M. S. Wrighton and C. M. Lieber, *J. Am. Chem. Soc.*, 1995, **117**, 7943.
5 S. K. Sinniah, A. B. Steel, C. J. Miller and J. E. Reutt-Robey, *J. Am. Chem. Soc.*, 1996, **118**, 8925.
6 R. McKendry, M. E. Theoclitou, T. Rayment and C. Abell, *Nature*, 1998, **391**, 566.
7 S.-T. Yau, B. R. Thomas and P. G. Vekilov, *Phys. Rev. Lett.*, 2000, **85**, 353.
8 K. Tsuchie, T. Nagao and S. Hasegawa, *Phys. Rev. B*, 1999, **60**, 11 131.
9 T. W. Fishlock, A. Oral, R. G. Egdell and J. B. Pethica, *Nature*, 2000, **404**, 743.
10 R. M. Barrer, J. W. Baynham. F. W. Bultitude and W. M. Meier, *J. Chem. Soc.*, 1959, 195.
11 M. T. Weller, *J. Chem. Soc., Dalton Trans.*, 2000, 4227 and refs. cited therein.
12 C. T. Kresge, M. E. Leonowicz, W. J. Roth, J. C. Vartuli and J. S. Beck, *Nature*, 1992, **359**, 710.
13 B. J. Scott, G. Wirnsberger and G. D. Stucky, *Chem. Mater.*, 2001, **13**, 3140.
14 W. M. Meier, D. H. Olson and Ch. Baerlocher, *Atlas of Zeolite Structures*, Elsevier, Amsterdam, 4th edn., 1996.
15 W. Zhou, J. M. Thomas, D. S. Shephard, B. F. G. Johnson, T. Maschmeyer, R. G. Bell and Q. Ge, *Science*, 1998, **280**, 705.
16 Z. Zhang, D. Gekhtman, M. S. Dresselhaus and J. Ying, *Chem. Mater.*, 1999, **11**, 1659.
17 B. H. Hong, S. C. Bae, C.-W. Lee, S. Jeong and K. S. Kim, *Science*, 2001, **294**, 348.
18 H. Ohnishi, Y. Kondo and K. Takayanagi, *Nature*, 1998, **395**, 780.
19 Y. Kondo and K. Takayamagi, *Science*, 2000, **289**, 606.
20 S. Iijima and T. Ichihashi, *Nature*, 1993, **363**, 603.
21 D. S. Bethune, C. H. Kiang, M. S. de Vries, G. Gorman, R. Savoy, J. Vazquez and R. Beyers, *Nature*, 1993, **363**, 605.
22 P. M. Ajayan, J. M. Lambert, P. Bernier, L. Barbedette, C. Colliex and J. M. Planeix, *Chem. Phys. Lett.*, 1993, **215**, 509.
23 T. Guo, P. Nikolaev, A. Thess, D. T. Colbert and R. E. Smalley, *Chem. Phys. Lett.*, 1995, **243**, 49.
24 P. Nikolaev, M. J. Bronikowski, R. K. Bradley, F. Rohmund, D. T. Colbert, K. A. Smith and R. E. Smalley, *Chem. Phys. Lett.*, 1999, **313**, 91.
25 J. Sloan, M. C. Novotny, S. R. Bailey, G. Brown, C. Xu, V. C. Williams, S. Friedrichs, E. Flahaut, R. L. Callendar, A. P. E. York, K. S. Coleman, M. L. H. Green, R. E. Dunin-Borkowski and J. L. Hutchison, *Chem. Phys. Lett.*, 2000, **329**, 61.
26 R. R. Meyer, J. Sloan, R. E. Dunin-Borkowski, A. I. Kirkland, M. C. Novotny, S. R. Bailey, J. L. Hutchison and M. L. H. Green, *Science*, 2000, **289**, 1324.
27 J. Sloan and M. L. H. Green, in *Fullerenes: Chemistry, Physics and Technology*, K.M. Kadish and R.S. Ruoff, ed., Wiley Interscience, New York, 2000, p. 795.
28 C. Xu, J. Sloan, G. Brown, S. R. Bailey, V. C. Williams, S. Friedrichs, K. S. Coleman, E. Flahaut, J. L. Hutchison, R. E. Dunin-Borkowski and M. L. H. Green, *Chem. Commun.*, 2000, 2427.
29 J. Sloan, S. Grosvenor, S. R. Friedrichs, A. I. Kirkland, J. L. Hutchison and M. L. H. Green, *Angew. Chem., Int. Ed.*, 2002, **114**, 1204.
30 J. Sloan, J. Hammer, M. Zweifka-Sibley and M. L. H. Green, *Chem. Commun.*, 1998, 347.
31 S. C. Tsang, P. J. F. Harris and M. L. H. Green, *Nature*, 1993, **362**, 520.
32 S. C. Tsang, Y. K. Chen, P. J. F. Harris and M. L. H. Green, *Nature*, 1994, **372**, 159.
33 P. M. Ajayan and S. Iijima, *Nature*, 1993, **361**, 6410.
34 P. M. Ajayan, O. Stephan, P. Redlich and C. Colliex, *Nature*, 1995, **375**, 564.
35 J. Sloan, D. M. Wright, H. G. Woo, S. Bailey, G. Brown, A. P. E. York, K. S. Coleman, J. L. Hutchison and M. L. H. Green, *Chem. Commun.*, 1999, 699.
36 T. W. Ebbesen, *J. Phys. Chem. Solids*, 1996, **57**, 951.
37 C. H. Kiang, J.-S. Choi, T. T. Tran and A. D. Bacher, *J. Phys. Chem. B*, 1999, **103**, 7449.
38 G. Brown, S. R. Bailey, J. Sloan, C. Xu, S. Friedrichs, E. Flahaut, K. S. Coleman, M. L. H. Green, J. L. Hutchison and R. E. Dunin-Borkowski, *Chem. Commun.*, 2001, 845.
39 J. Mittal, M. Monthioux, H. Allouche and O. Stephan, *Chem. Phys. Lett.*, 2001, **339**, 311.
40 S. Friedrichs, R. R. Meyer, J. Sloan, A. I. Kirkland, J. L. Hutchison and M. L. H. Green, *Chem. Commun.*, 2001, 929.
41 S. Friedrichs, J. Sloan, M. L. H. Green, J. L. Hutchison, R. R. Meyer and A. I. Kirkland, *Phys. Rev. B*, 2001, **64**, 045406/1.
42 X. Fan, E. C. Dickey, P. C. Eklund, K. A. Williams, L. Grigorian, R. Buczko, S. T. Pantelides and S. J. Pennycook, *Phys. Rev. Lett.*, 2000, **84**, 4621.
43 B. W. Smith, M. Monthioux and D. E. Luzzi, *Nature*, 1998, **396**, 323.
44 J. Sloan, R. E. Dunin-Borkowski, J. L. Hutchison, K. S. Coleman, V. C. Williams, J. B. Claridge, A. P. E. York, C. Xu, S. R. Bailey, G. Brown, S. Friedrichs and M. L. H. Green, *Chem. Phys. Lett.*, 2000, **316**, 191.
45 Y. Zhang, S. Iijima, Z. Shi and Z. Gu, *Philos. Mag. Lett.*, 1999, **79**, 473.
46 B. W. Smith, D. E. Luzzi and Y. Achiba, *Chem. Phys. Lett.*, 2000, **331**, 137.
47 K. Suenaga, M. Tence, C. Mory, C. Colliex, H. Kato, T. Okazaki, H. Shinohara, K. Hirahara, S. Bandow and S. Iijima, *Science*, 2000, **290**, 2280.
48 J. Sloan, M. Terrones, S. Nufer, S. Friedrichs, S. R. Bailey, H. G. Woo, M. Rühle, J. L. Hutchison and M. L. H. Green, *J. Am. Chem. Soc.*, 2002, **124**, 2116.
49 J. Sloan, J. Cook, A. Chu, M. Zwiefka-Sibley, M. L. H. Green and J. L. Hutchison, *J. Solid State Chem.*, 1998, **140**, 83.
50 B. W. Smith and D. E. Luzzi, *Chem. Phys. Lett.*, 2000, **321**, 169.
51 K. Hirahara, K. Suenaga, S. Bandow, H. Kato, T. Okazaki, H. Shinohara and S. Iijima, *Phys. Rev. Lett.*, 2000, **85**, 5384.
52 K. Hirahara, S. Bandow, K. Suenaga, H. Kato, T. Okazaki, H. Shinohara and S. Iijima, *Phys. Rev. B*, 2001, **64**, 115 420–1.
53 A. F. Wells, in *Structural Inorganic Chemistry*, Oxford University Press, Oxford, 5th edn., 1990, p. 409.
54 J. Sloan, G. Brown, S. R. Bailey, K. S. Coleman, E. Flahaut, S. Friedrichs, C. Xu, M. L. H. Green, R. E. Dunin-Borkowski, J. L. Hutchison and A. I. Kirkland, in *Proceedings of the Fall 2000 MRS*, Materials Research Society, Boston, MA, 2000, **vol. 633**, A14.31.
55 J. Sloan, S. Friedrichs, R. R. Meyer, A. I. Kirkland, J. L. Hutchison and M. L. H. Green, *Inorg. Chim. Acta*, 2002, **330**, 1.
56 R. R. Meyer, A. I. Kirkland and W. O. Saxton, *Ultramicroscopy*, in press.
57 M. Wilson and P. A. Madden, *J. Am. Chem. Soc.*, 2001, **123**, 2101.
58 The conformation and diameter of a SWNT are effectively specified by (*n*,*m*) where *n* and *m* are integers in the equation $\boldsymbol{C}_\mathbf{h} = n\boldsymbol{a}_1 + m\boldsymbol{a}_2$, where $\boldsymbol{C}_\mathbf{h}$ is the 'roll-up' vector of the nanotube and $\boldsymbol{a}_1$ and $\boldsymbol{a}_2$ are the basal vectors of the parent sp^2 graphene lattice. See also: M. S. Dresselhaus, G. Dresselhaus and R. Saito, *Carbon*, 1995, **33**, 883.
59 J. L. Hutchison, R. C. Doole, R. E. Dunin-Borkowski, J. Sloan and M. L. H. Green, *JEOL News*, 1999, **34E**, 10.
60 K. F. Mucker, G. S. Smith, Q. Johnson and R. E. Elson, *Acta Crystallogr., Sect. B*, 1969, **25**, 2362; see also ref. 53, p. 426.
61 E. B. Brackett and T. E. Brackett, *J. Phys. Chem.*, 1963, **67**, 2132.
62 H. P. Beck, *J. Solid State Chem.*, 1983, **47**, 328.
63 J. M. Léger, J. Haines and A. Atouf, *J. Appl. Crystallogr.*, 1995, **28**, 416.
64 F. Banhart, *Rep. Prog. Phys.*, 1999, **62**, 1181.
65 B. W. Smith and D. E. Luzzi, *J. Appl. Phys.*, 2001, **90**, 3509.
66 C. R. A. Catlow, K. M. Diller and L. W. Hobbs, *Philos. Mag. A*, 1980, **42**, 123.
67 M. L. Jenkins and M. A. Kirk, in *Characterisation of Radiation Damage by Transmission Electron Microscopy*, Institute of Physics, Bristol, 2000, p. 173.
68 G. C. Fryburg and R. A. Lad, *Surf. Sci.*, 1975, **48**, 353.
69 B. Krebs, *Angew. Chem.*, 1969, **81**, 120.
70 T. Okazaki, K. Suenaga, H. Kazutomo, S. Bandow, S. Iijima and H. Shinohara, *J. Am. Chem. Soc.*, 2001, **123**, 9673.
71 E. Philp, J. Sloan, S. Friedrichs, A. I. Kirkland, R. Meyer, J. L. Hutchison and M. L. H. Green, manuscript in preparation.
72 H. W. Kroto, J. R. Heath, S. C. Obrien, R. F. Curl and R. E. Smalley, *Nature*, 1985, **318**, 162.